Carbohydrate Polymers 117 (2015) 549–558

Contents lists available at ScienceDirect

Carbohydrate Polymers

journal homepage: www.elsevier.com/locate/carbpol

Amorphous nanodrugs prepared by complexation with polysaccharides: Carrageenan versus dextran sulfate

Wean Sin Cheow, Tie Yi Kiew, Kunn Hadinoto*

School of Chemical and Biomedical Engineering, Nanyang Technological University, 62 Nanyang Drive, Singapore 637459, Singapore

ARTICLE INFO

Article history:
Received 12 July 2014
Received in revised form
28 September 2014
Accepted 12 October 2014
Available online 23 October 2014

Keywords:
Polysaccharide nanoparticles
Drug-polysaccharide complex
Nanomedicine
Colloidal polysaccharides
Supersaturated drug delivery system

ABSTRACT

Amorphous nanodrugs prepared by electrostatic complexation of drug molecules with oppositely charged polysaccharides represent a promising bioavailability enhancement strategy for poorly-soluble drugs owed to their high supersaturation generation capability and simple preparation. Using ciprofloxacin (CIP) as the model drug, we investigated the effects of using dextran sulfate (DXT) or carrageenan (CGN) on the (1) preparation efficiency, (2) physical characteristics, (3) supersaturation generation, (4) antimicrobial activity, and (5) cytotoxicity of the amorphous drug-polysaccharide nanoparticle complex (nanoplex) produced. Owing to the higher charge density and chain flexibility of DXT, coupled with the greater hydrophobicity of CGN, the CIP–DXT nanoplex exhibited superior preparation efficiency and larger size than the CIP–CGN nanoplex. Whereas the low solubility and high gelation tendency of CGN resulted in superior supersaturation generation capability for the CIP–DXT nanoplex. The non-cytotoxicity, antimicrobial activity, colloidal, and amorphous state stability were established for both nanoplexes, making them an ideal supersaturated drug delivery system.

1. Introduction

Amorphous drug nanoparticles (or nanodrugs in short) represent a provenly effective oral bioavailability enhancement strategy for poorly-soluble drugs attributed to the amorphous nanodrugs' ability to generate a highly supersaturated drug concentration, resulting in significantly higher apparent drug solubility compared to their crystalline or amorphous drug microparticle counterparts (Matteucci et al., 2007). The excellent supersaturation generation ability of the amorphous nanodrugs is attributed to (1) the metastable state of the amorphous form and (2) the fast drug dissolution rate afforded by the large specific surface area of the nanoparticles (Lindfors et al., 2006). The high apparent drug solubility in turn enhances the drug bioavailability provided that the high supersaturation level is maintained over a period sufficient for the drug absorption across the gastrointestinal lumen to occur (Alonzo, Zhang, Zhou, Gao, & Taylor, 2010).

While the supersaturation generation capability of amorphous nanodrugs has been widely acknowledged, their implementation as solid dosage form of poorly soluble drugs has been hindered by their intricate preparation, which requires in situ suppression of the particle growth while simultaneously stabilizing the amorphous state. Various preparation techniques of amorphous nanodrugs have been proposed, for example by antisolvent precipitation (Matteucci et al., 2007), sonoprecipitation (Dhumal, Biradar, Yamamura, Paradkar, & York, 2008), and pH-shift precipitation (Mou, Chen, Wan, Xu, & Yang, 2011). These proposed techniques, however, are lacking in their feasibility because of one or more of the following issues, i.e. high energy expense, heavy use of solvents, poor scalability, high material wastage, or low throughput.

For this reason, we developed in a previous study an alternative preparation technique of amorphous nanodrugs by electrostatic complexation of charged drug molecules with oppositely charged polysaccharides (Cheow & Hadinoto, 2012). This technique is simple in practice, where it involves only mixing of the drug and polysaccharide solutions under ambient condition, resulting in minimal energy expense. The technique is also solvent free, readily scalable owed to its simple operating principle, cost effective due to the abundance of polysaccharides, and exhibits a high drug utilization rate, thus minimal drug wastage.

Abbreviations: ATCC, American Type Culture Collection; CE, complexation efficiency; CFU, colony forming unit; CGN, carrageenan; IP, ciprofloxacin; DMEM, Dulbecco's modified Eagle's medium; DMSO, dimethyl sulfoxide; DSC, differential scanning calorimetry; DXT, dextran sulfate; EDTA, ethylenediaminetetraacetic acid; FESEM, field emission scanning electron microscope; HPMC, hydroxypropyl methylcellulose; MHB, Mueller Hinton broth; MIC, minimum inhibitory concentration; MTT, (3-(4,5-dimethylthiazol-2-yl)-2,5-diphenyltetrazolium bromide); MW, molecular weight; PBS, phosphate buffer saline; PTFE, polytetrafluoroethylene; PXRD, powder x-ray diffraction; TGA, thermogravimetric analysis.

* Corresponding author. Tel.: +65 6514 8381; fax: +65 6794 7553.
E-mail address: kunnong@ntu.edu.sg (K. Hadinoto).

http://dx.doi.org/10.1016/j.carbpol.2014.10.015
0144-8617/

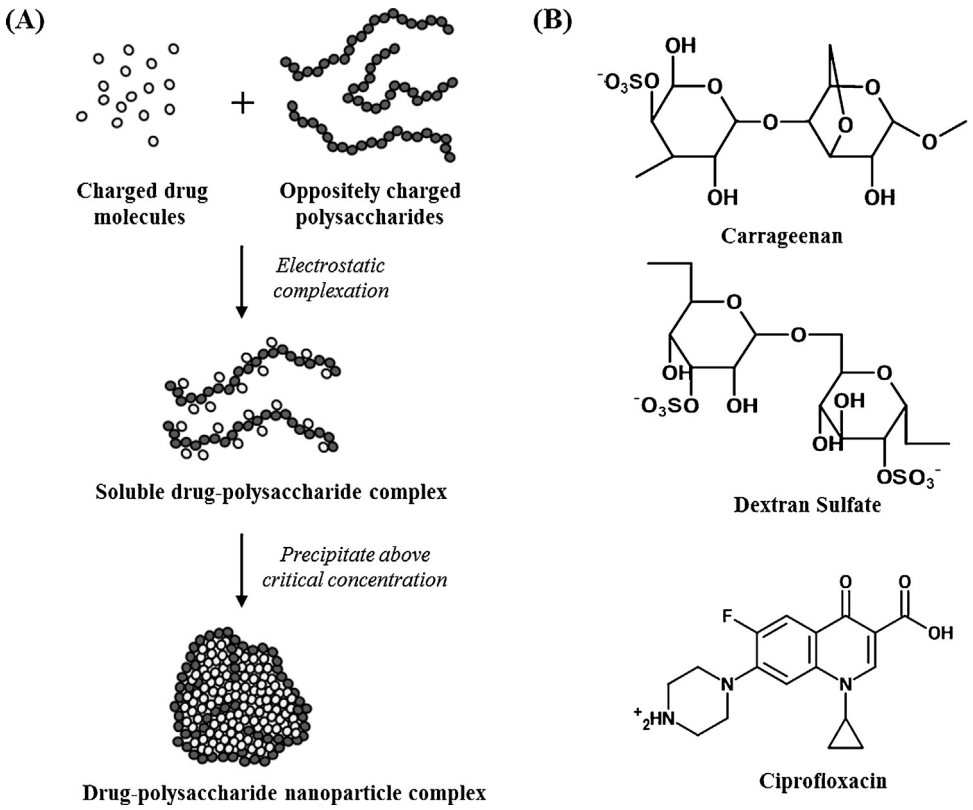

Fig. 1. (A) Electrostatically-driven complexation between drug molecules and oppositely charged polysaccharides resulting in the formation of drug-polysaccharide nanoparticle complex (nanoplex); (B) electrostatic interactions between the nitro group of ciprofloxacin (CIP) and the sulfate groups of carrageenan (CGN) and dextran sulfate (DXT).

In this technique, ionized drug molecules in acid or base are mixed with oppositely charged polysaccharides in the presence of salt, to form soluble drug-polysaccharide complex, as illustrated in Fig. 1A. The role of salt is to reduce the repulsions between the like charges of the polysaccharide chains, which prevent the chain rearrangement and compaction that are necessary for the complex formation (Caram-Lelham, Hed, & Sundelof, 1997). Owing to the hydrophobic interactions between the drug molecules, aggregates of the drug-polysaccharide complex are subsequently formed. The aggregates eventually precipitate out to form the drug-polysaccharide nanoparticle complex (or drug nanoplex in short) upon reaching a critical aggregate concentration, whose value is mostly governed by the hydrophobicity of the drug and polysaccharides. The strong electrostatic interactions between the drug and polysaccharides prevent the drug molecules from assembling into ordered crystalline structures upon their precipitation, resulting in the amorphous state.

The strong electrostatic drug-polysaccharide interactions also play important roles after preparation. First, they stabilize the amorphous state of the drug nanoplex by restricting the drug molecular mobility, hence reducing the crystallization propensity of the amorphous state during storage and dissolution. Second, they contribute to the generation of a sustained supersaturation level as the drug molecules can only be released upon their decomplexation from the polysaccharides in the presence of electrolytes, as opposed to burst dissolution of drug molecules in conventional amorphous nanodrugs (Sun & Lee, 2013). On this note, amorphous drug nanoplex has been found to exhibit a more prolonged supersaturation level and higher amorphous state stability than amorphous nanodrugs prepared by pH-shift precipitation (Cheow, Kiew, Yang, & Hadinoto, 2014).

In contrast to polysaccharide nanoparticle complex encapsulating drug, which is prepared by complexation of two oppositely charged polysaccharides and in which the drug is molecularly dispersed in the polysaccharide matrix (Ramasamy et al., 2014), the amorphous drug nanoplex is made up largely of the drug itself, resulting in the high drug loading. Herein the primary roles of the polysaccharides are to provide colloidal and amorphous state stability for the nanoplex, instead of acting as drug carriers like in the polysaccharide nanoparticle complex. Even though the drug-polysaccharide complexation technique requires the poorly soluble drugs to be soluble in acid or base, this should not hinder its pervasive application as a majority of drugs are weak organic acids or bases (Ando & Radebaugh, 2005).

The amorphous drug nanoplex, however, thus far has only been prepared and evaluated using one polysaccharide, i.e. anionic dextran sulfate (DXT). Herein we extend the investigation to a different anionic polysaccharide, i.e. κ-carrageenan (CGN), using antibiotic ciprofloxacin (CIP) as the model poorly soluble cationic drugs. In this regard, both DXT and CGN have been extensively used in drug delivery formulations as materials for extended release tablet, encapsulation, and extrusion lubricant (Delair, 2011; Li, Ni, Shao, & Mao, 2014). They are both sulfated polysaccharides, thereby their $-SO_3^-$ can readily interact with the $-NH_2^+$ group of CIP to form the CIP nanoplex, as shown in Fig. 1B. Nevertheless, DXT and CGN are distinct in several properties that have been known to have important roles in the drug-polysaccharide complexation, such as charge density, chain flexibility, and gelation tendency.

Specifically, CGN possesses a lower chain flexibility parameter (B) compared to DXT at 0.11 and 0.23 for CGN and DXT, respectively (Caram-Lelham et al., 1997), whereas the persistence lengths of the CGN and DXT chains are 6.8 nm (Slootmaekers, Dejonghe, Reynaers, Varkevisser, & Vantreslong, 1988) and 1.6 nm (Schatz, Domard, Viton, Pichot, & Delair, 2004), respectively. The lower chain flexibility parameter and the greater persistence length of the CGN chains signify their greater stiffness, which indicates that repulsions of the

like-charged polyanionic chains in CGN are less responsive to the charge shielding effect of the salt.

As a result, the CGN chains have a higher tendency to remain in their extended form compared to the DXT chains in the presence of salt. When the polysaccharide chains are in their extended form, there is a longer distance between the charged groups, resulting in essentially lower charge densities locally. As the nanoplex formation depends on the ability of the polysaccharide chains to attract the oppositely charged drug molecules, the difference in the chain flexibility between CGN and DXT is expected to have an impact on the nanoplex formation.

Furthermore, unlike DXT, CGN has a unique ability to bind a large amount of water to form a gel network (Kara, Tamerler, & Pekcan, 2003). The presence of gel around the nanoplex can influence the ability of the drug molecules to decomplex from the CGN chains in the presence of electrolytes, as well as the ability of the drug molecules to diffuse out after the decomplexation. Thus, in addition to their anticipated impacts on the nanoplex formation, the variations in the properties between DXT and CGN are anticipated to also influence the resultant nanoplex characteristics, such as its stability and supersaturation generation capability.

Therefore, the objectives of the present work are to compare the CIP–DXT and CIP–CGN nanoplexes in terms of their (1) preparation efficiency, (2) physical characteristics (i.e. morphology, amorphous state stability, colloidal stability, and powder flowability), (3) supersaturation generation capability, (4) in vitro antimicrobial activity against *Escherichia coli* (*E. coli*) bacteria, and (5) in vitro cytotoxicity towards human epithelium cells. From these comparisons, the effects of the polysaccharide properties on the nanoplex preparation and its resultant characteristics are elucidated. As the CIP–CGN nanoplex were prepared for the first time, the influences of different process variables on the CIP–CGN nanoplex preparation were presented first.

2. Materials

Materials for CIP nanoplex preparation: Ciprofloxacin (CIP), sodium chloride (NaCl), glacial acetic acid, mannitol, hydroxypropyl methylcellulose (HPMC), phosphate buffer saline (PBS, pH 7.4), and κ-carrageenan (CGN) with molecular weight (MW) of 50 kDa and viscosity of 5–25 mPa s at 0.3% (w/v) in 25 °C water were purchased from Sigma–Aldrich (USA). Dextran sulfate (DXT, MW 5 kDa) was purchased from Wako Pure Chemical (Japan). ***Materials for antimicrobial activity test***: *E. coli* W3110 strain and Mueller–Hinton broth (MHB) were purchased from American Type Culture Collection (ATCC, USA) and BD Diagnostics (USA), respectively. ***Materials for cytotoxicity test***: A549 adenocarcinomic human alveolar basal epithelial cells were purchased from ATCC (USA). (3-(4,5-dimethylthiazol-2-yl)-2,5-diphenyltetrazolium bromide) (MTT, 98% purity), 0.25% trypsin- ethylenediaminetetraacetic acid (EDTA) solution, penicillin-streptomycin, and dimethyl sulfoxide (DMSO) were purchased from Alfa Aesar (United Kingdom), Gibco (Canada), PAA Laboratories (Austria), and Sigma–Aldrich (USA), respectively. Dulbecco's modified Eagle's medium (DMEM) and fetal bovine serum were purchased from HyClone (Thermo Scientific, USA).

3. Methods

3.1. Preparation of CIP nanoplex

3.1.1. CIP–CGN nanoplex

CIP–CGN nanoplex was prepared at a constant CIP concentration of 10 mg/mL while the charge ratio of CIP to CGN ($R_{CIP/CGN}$) was varied from 0.4 to 2.0. The $R_{CIP/CGN}$ was calculated from charge densities of CIP and CGN, which were equal to 3.0×10^{-6} (Cheow & Hadinoto, 2012) and 2.3×10^{-6} mol charge/mg (Hugerth & Sundelof, 2001), respectively. Briefly, CIP was dissolved at 10 mg/mL in 0.3% (v/v) acetic acid, while a variable amount of CGN (according to the intended $R_{CIP/CGN}$) was dissolved in 0.1 M or 0.3 M NaCl at 60 °C. The CIP solution was then added under gentle stirring to the CGN solution, whose temperature was maintained at 60 °C in a water bath. The mixture was let sit in the water bath for 30 min for the complexation to equilibrate. Afterwards, the CIP–CGN nanoplex was recovered by three cycles of centrifugation and washing at 14,000 × *g* and 20 min, followed by re-suspension of the nanoplex in deionized water.

3.1.2. CIP–DXT nanoplex

CIP–DXT nanoplex was prepared at a charge ratio of CIP to DXT ($R_{CIP/DXT}$) equal to 1.3, which was found to produce the optimal preparation efficiency in Cheow and Hadinoto (2012). Briefly, CIP was dissolved at 10 mg/mL in 0.2% (v/v) acetic acid, whereas DXT, whose charge density was equal to 4.8×10^{-6} mol charge/mg, was dissolved at 4.5 mg/mL in deionized water containing 5.8 mg NaCl. The CIP solution was then added under gentle stirring into the DXT solution under ambient condition. The mixture was let sit for 30 min after which the CIP–DXT nanoplex was recovered by three cycles of centrifugation and washing at 13,000 × *g* and 20 min, followed by re-suspension of the nanoplex in deionized water.

3.2. Preparation efficiency

The efficiency of the nanoplex preparation was evaluated in terms of (1) the CIP complexation efficiency, (2) yield, and (3) CIP loading. First, the complexation efficiency (CE), which was defined as the mass percentage of CIP initially added that was transformed into the nanoplex, was determined from the amount of free CIP recovered in the supernatant of the mixed solution of CIP and polysaccharides after the first centrifugation and washing cycle. The amount of CIP in the supernatant was quantified by UV–vis spectrophotometer (UV Mini-1240, Shimadzu, Japan) at absorbance wavelength of 324 nm. On this note, for both the CIP–DXT and CIP–CGN nanoplexes, the non-complexed CIP was completely removed from the nanoplex suspension after the three cycles of centrifugation and washing, as confirmed by CIP concentration measurement in the supernatant after the third cycle by UV–vis spectrophotometer.

Second, the yield, which was defined as the mass ratio of the nanoplex produced to the amount of CIP and polysaccharides initially added, was determined by freeze drying an aliquot of the nanoplex suspension in Alpha 1–2 LD Plus freeze dryer (Martin Christ, Germany). Third, the CIP loading, which was defined as the mass percentage of CIP in the nanoplex (with the rest being the polysaccharides), was determined from the total amount of CIP released measured by UV–vis spectrophotometer after a complete dissolution of a known mass of nanoplex in PBS. The reported CE, yield, and CIP loading were obtained from three independent replicates performed on different days.

3.3. Physical characterizations

Physical characteristics of the nanoplex were evaluated in terms of (1) the morphology (i.e. size, shape), (2) colloidal stability, (3) amorphous state stability, and (4) powder flowability after freeze drying. The morphology was characterized by Field Emission Scanning Electron Microscope (FESEM) model JSM-6700F (JEOL, USA) in which the sample was sputter coated with platinum. The size was determined from the FESEM images using ImageJ software (NIH, USA) based on two hundred particle counts. The colloidal stability was characterized by the zeta potential, which was measured in triplicates by Brookhaven 90Plus Zeta Sizer (Brookhaven

Instruments Corporation, USA) using the principle of dynamic light scattering.

The amorphous state stability of the nanoplex after six months storage at 25 °C and relative humidity of 55% was evaluated by Powder X-Ray Diffraction (PXRD) using D8 Advance X-ray diffractometer equipped with Cu $K\alpha$ radiation (Bruker, Germany) from 10° to 60° (2θ) with a step size of 0.02°/s. The amorphous state stability was also examined by differential scanning calorimetry (DSC)/thermogravimetric analysis (TGA) from 25 °C to 300 °C at a heating rate of 10 °C/min using DSC 822e (Mettler Toledo, USA). The nanoplex was transformed into dry powders by 24-h freeze drying with mannitol at 1:1 ratio, where the water-soluble mannitol functioned as interstitial excipient bridges to prevent irreversible agglomeration of the nanoplex upon drying.

The flowability of the nanoplex after freeze drying was characterized by the Carr's Index (Eq. (1)), where Carr's Index ≤21 indicates good flowability and Carr's Index ≥33 indicates poor flowability (Zheng, 2009). The bulk density (ρ_{bulk}) in Eq. (1) was determined from the measured volume of a known mass of the freeze-dried nanoplex without tapping, whereas the tap density (ρ_{tap}) was determined in triplicates after 2000 taps using tap densitometer (Quantachromme, USA).

$$\text{Carr's index} = \left(1 - \frac{\rho_{bulk}}{\rho_{tap}}\right) \times 100\% \quad (1)$$

3.4. Supersaturation generation

The supersaturation generation capability of the nanoplex was evaluated in their aqueous suspension and dry powder forms in the presence of HPMC, which is known for its crystallization inhibiting capability. Herein the roles of HPMC were to inhibit the solution-mediated crystallization of the dissolved drug, while simultaneously impeding the Ostwald ripening growth of the remaining solid phase undergoing dissolution, thereby maintaining the supersaturated condition (Tajarobi, Larsson, Matic, & Abrahmsen-Alami, 2011). For the nanoplex powders, the supersaturation generation was evaluated in the presence of dissolved or dry powder HPMC, where the latter was intended to simulate HPMC's physical existence in actual drug solid dosage forms (e.g. tablets).

The saturation solubility (C_{eq}) of CIP was determined first by incubating native crystalline CIP in excess in 20 mL PBS at 37 °C for 24 h. Afterwards, the native CIP solution was centrifuged and filtered. CIP concentration in the filtered solution was then quantified by UV–vis spectrophotometer at wavelength of 324 nm from which C_{eq} was obtained. The supersaturated CIP solution was generated by adding the nanoplex in excess into 8.5 mL PBS at 37 °C in a shaking incubator. Afterwards, 0.2 mL aliquot was withdrawn at fixed time intervals over a 4-h period. The aliquot was filtered immediately using 0.22 μm PTFE membranes and diluted tenfold with fresh PBS to prevent CIP precipitation from the supersaturated solution. The CIP concentration in the aliquot was quantified by UV–vis spectrophotometer to determine the supersaturated CIP concentration (C) from which the supersaturation level, defined as the ratio of C to C_{eq}, was determined.

The rate of supersaturation generation of the nanoplex was characterized from the dissolution rate of CIP from the nanoplex under sink condition. Briefly, the nanoplex (1.5 mg for the aqueous suspension and 3.0 mg for dry powders) was immersed in a dialysis bag in 12 mL PBS in a shaking incubator at 37 °C. At fixed time intervals over a 4-h period, 2 mL aliquot was withdrawn and replenished with fresh PBS of the same volume. CIP concentration in the aliquot was then quantified in triplicates by UV–vis spectrophotometer. The reported supersaturation generation was obtained from three independent replicates performed on different days.

3.5. Antimicrobial activity

Antimicrobial activity of the nanoplex was evaluated from its minimum inhibitory concentration (MIC) against planktonic cells of *E. coli* bacteria. The MIC was defined as the lowest CIP concentration capable of suppressing visible bacterial growth after overnight incubation at 37 °C. Optical density of the bacterial suspension at 600 nm (OD_{600}) was used to gauge the extent of bacterial growth, where $OD_{600} < 1$ signified zero visible bacterial growth. Bacterial suspension of *E. coli* used as the inoculum was adjusted to 0.5 McFarland standard in Mueller Hinton broth (MHB) and subsequently diluted 100-fold to produce cell suspension having 10^6 colony forming units (CFU)/mL.

The MIC was determined by broth microdilution in a 96-well microplate using CIP solutions generated from the dissolution of the nanoplex in PBS. Briefly, 5 μL CIP solution was added to 95 μL MHB followed by serial twofold dilutions to produce CIP solutions having concentrations of 1 to 0.0005 μg/mL. Next, 100 μL of the cell suspension was added to the microplate wells containing the CIP solution and incubated at 37 °C for 24 h. Wells without CIP and without the cells were used as the positive and negative controls, respectively. Afterwards, OD_{600} of the cell suspension in each microplate well was measured using a microplate reader (Synergy HT, Biotek, USA). The lowest CIP concentration that resulted in $OD_{600} < 0.1$ was determined to be the MIC using two biological replicates and three technical replicates.

3.6. Cytotoxicity

The cytotoxicity of the nanoplex towards the A549 cells was evaluated in vitro using the MTT assay following the protocol of Vandeloosdrecht, Beelen, Ossenkoppele, Broekhoven, and Langenhuijsen (1994). Briefly, the A549 cells were cultivated in DMEM supplemented with 10% (w/v) fetal bovine serum and 1% (w/v) penicillin-streptomycin solution at a density of 10^5 cells/well in a 24-well plate. After 24 h incubation at 37 °C in a 5% CO_2 incubator, the cells were treated with the nanoplex and suspended in the supplemented DMEM for a further 24 h. The cytotoxicity was evaluated in triplicates at three different CIP concentrations (i.e. 0.5, 1.0, and 2.0 mg/mL). Wells containing only the cells and supplemented medium were used as the control.

Following the treatment with the nanoplex, the medium containing the nanoplex was replaced with serum-free DMEM containing 100 μL of MTT dye solution (0.5% w/v in PBS). After a further incubation for 4 h at 37 °C in a 5% CO_2 incubator, 2 mL of DMSO was added to dissolve the formazan crystals produced by the enzymatic reduction of MTT by the viable cells. The plate was gently shaken for 5 min at 100 RPM to ensure complete formazan dissolution. Formazan concentration was then determined by optical density measurement at 550 nm (OD_{550}) using UV–vis spectrophotometer. The cell survival was determined as a percentage of the formazan absorbance of the control by the ratio of OD_{550} of the treated cells to OD_{550} of the control.

4. Results and discussion

4.1. Preparation efficiency of CIP–CGN nanoplex

The preparation efficiency of the CIP–CGN nanoplex was evaluated as a function $R_{CIP/CGN}$ (i.e. 0.4, 0.6, 1.0, 1.3, 1.6, and 2.0) at two salt concentrations (i.e. NaCl = 0.1 and 0.3 M). At NaCl = 0.1 M, the CE was found to decrease with increasing $R_{CIP/CGN}$ from its maximum point of ≈75% at $R_{CIP/CGN} = 0.4$ to ≈22% at $R_{CIP/CGN} = 2.0$ (Fig. 2A). As CIP concentration was kept constant in this study, there was abundant CGN available for electrostatic complexation with the

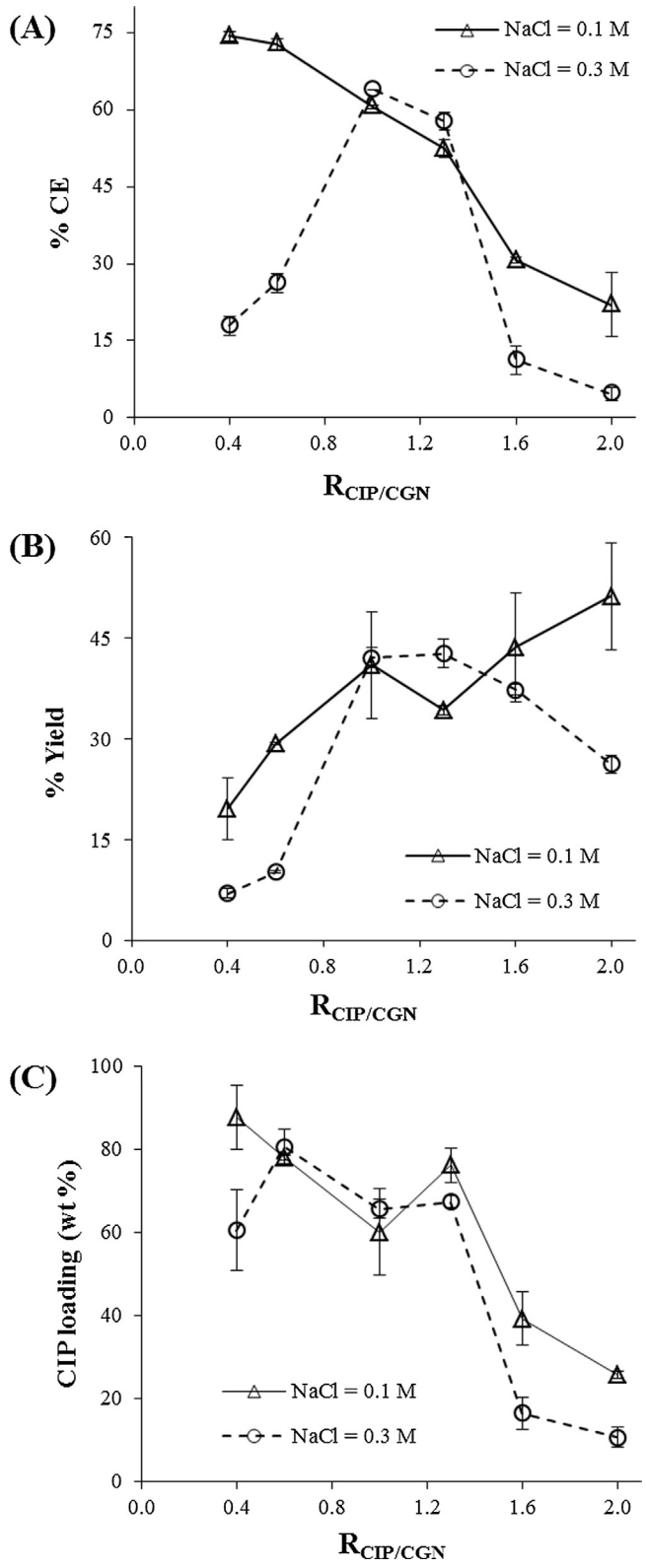

Fig. 2. Preparation efficiency of CIP–CGN nanoplex were evaluated as a function of $R_{CIP/CGN}$ at two NaCl concentration in terms of the (A) complexation efficiency (CE), (B) yield, and (C) CIP loading, from which $R_{CIP/CGN}$ in the vicinity of 1.0 at NaCl = 0.1 M was determined to be optimal.

CIP molecules at low $R_{CIP/CGN}$ (<1.0), resulting in the higher CE. As $R_{CIP/CGN}$ increases, however, fewer CGN was present resulting in the lower CE, particularly for $R_{CIP/CGN} > 1.0$.

A different trend in the CE variation as a function of $R_{CIP/CGN}$, however, was observed at NaCl = 0.3 M (Fig. 2A). At $R_{CIP/CGN} = 0.4$, the CE was ≈18% after which it increased gradually as $R_{CIP/CGN}$ was raised, until it reached a plateau at ≈63% for $R_{CIP/CGN} = 1.0$. When $R_{CIP/CGN}$ was raised further to above 1.0, the CE decreased sharply to ≈5% at $R_{CIP/CGN} = 2.0$ due to insufficient CGN available for complexation. Overall, the CEs at NaCl = 0.3 M were considerably lower than the CEs at NaCl = 0.1 M, with the exception of $R_{CIP/CGN} = 1.0$ and 1.3, where the CEs were found to be comparable between the two salt concentrations. The lower CEs at NaCl = 0.3 M for $R_{CIP/CGN} \ll 1$ and $R_{CIP/CGN} \gg 1$ was caused by the stronger charge shielding effect of the salt, which made it more difficult for the CIP molecules to interact electrostatically with the CGN chains. The same trend was reported for the CIP–DXT nanoplex across all $R_{CIP/DXT}$ by Cheow and Hadinoto (2012).

The non-conformance to this trend at $R_{CIP/CGN} = 1.0$ and 1.3, where there were roughly the same amount of CIP and CGN's molecular charges present, suggested that the interaction between CIP and CGN at these $R_{CIP/CGN}$ values was cooperative in nature. In other words, at $R_{CIP/CGN} = 1.0$ and 1.3, the binding of a CIP molecule to available CGN sites encouraged the binding of other CIP molecules to aggregate at the same sites, primarily through hydrophobic interactions. As the hydrophobic aggregation of drug molecules has been known to be dominant over the drug-polysaccharide electrostatic interaction in cooperative bindings (Caram-Lelham et al., 1997), the effect of salt concentration, which influenced the drug-polysaccharide electrostatic interaction, on the CE was found to be minimal at $R_{CIP/CGN} = 1.0$ and 1.3.

In contrast to the CE trend, the yield at NaCl = 0.1 M was found to increase from ≈20% at $R_{CIP/CGN} = 0.4$ to ≈50% at $R_{CIP/CGN} = 2.0$, where the rate of increase was dampened for $R_{CIP/CGN} \geq 1.0$. Compared to the runs at $R_{CIP/CGN} \geq 1.0$, the lower yield at $R_{CIP/CGN} < 1.0$, which exhibited the higher CE (more nanoplex was produced), was caused by a large excess of CGN present in the feed that did not participate in the complexation with CIP. As the CIP concentration was held constant in this study, higher $R_{CIP/CGN}$ denoted less CGN available for complexation. Therefore, the fact that the yield changed only marginally as $R_{CIP/CGN}$ was raised for $R_{CIP/CGN} \geq 1.0$ suggested that the presumed decrease in the yield at high $R_{CIP/CGN}$ due to the fewer nanoplex produced was offset by an increase in the yield owed to the reduction in the non-utilized CGN with increasing $R_{CIP/CGN}$.

On the other hand, the increase in the yield as $R_{CIP/CGN}$ was raised for $0.4 \leq R_{CIP/CGN} \leq 1.0$ (despite the decreasing CE) hinted at an increase in the product formation, which was not necessarily owed to more CIP transforming into the nanoplex. The higher yield could be attributed to the higher CGN utilization rate as $R_{CIP/CGN}$ was raised, where more CGN was utilized to be part of the nanoplex resulting in a larger presence of CGN in the nanoplex produced. This resulted in the higher apparent yield despite fewer CIP was transformed into the nanoplex. This conjecture was supported by the CIP loading results at NaCl = 0.1 M shown in Fig. 2C, where the CIP loading was found to decrease with increasing $R_{CIP/CGN}$. Specifically, the CIP loading decreased from ≈88% at $R_{CIP/CGN} = 0.4$ to ≈60% at $R_{CIP/CGN} = 1.0$. In fact, the CIP loading continued to decrease to ≈25% as $R_{CIP/CGN}$ was raised above 1.0 due to the lower CE.

Relatively similar trends for the yield and CIP loading, where the former increased and the latter decreased as $R_{CIP/CGN}$ was raised, were observed at NaCl = 0.3 M. This was despite the variations in the CE trends between the two salt concentrations. One exception to these trends was the decrease in the yield with increasing $R_{CIP/CGN}$ for $R_{CIP/CGN} \geq 1.6$ at NaCl = 0.3 M, which was caused by the very low CEs (≈5–12%). Not unlike the CE, the yield and CIP loading

obtained at NaCl = 0.3 M were found to be lower than those obtained at NaCl = 0.1 M due to the stronger charge shielding effect of the salt.

On this note, the increase in the yield for $0.4 \leq R_{CIP/CGN} \leq 1.3$ as $R_{CIP/CGN}$ was raised at NaCl = 0.3 M was attributed to the increase in the CE that resulted in more nanoplex produced. However, the continued decrease in the CIP loading as $R_{CIP/CGN}$ was raised indicated that the higher CE obtained at higher $R_{CIP/CGN}$ was accompanied by a larger CGN presence in the nanoplex. This signified an increase in the CGN utilization rate at higher $R_{CIP/CGN}$, which was also observed at NaCl = 0.1 M. Thus, the higher CE coupled with the higher CGN utilization rate at higher $R_{CIP/CGN}$ contributed to the higher yield.

From the trends in the CE, yield, and CIP loading variations as a function of the salt concentration and $R_{CIP/CGN}$, it was concluded that (1) CIP–CGN nanoplex preparation at an excessive salt concentration (i.e. NaCl = 0.3 M) was ineffective as it suppressed the CIP–CGN electrostatic interaction, (2) low $R_{CIP/CGN}$ ($\ll 1.0$), while resulted in the highest CE and CIP loading, was not mass efficient due to the wastage of excess CGN resulting in the lowest yield, where on the other hand (3) high $R_{CIP/CGN}$ ($\gg 1.0$) resulted in the lowest CE and CIP loading due to insufficient CGN to undergo the complexation with CIP.

In addition, we learnt that the CGN utilization rate increased as $R_{CIP/CGN}$ was raised, which was independent of the trend in the CE. In other words, when there were fewer CGN present in the feed (i.e. high $R_{CIP/CGN}$), a larger portion of the CGN present participated in the complexation with CIP, resulting in the lower CIP loading, but higher yield. Based on these findings, it was determined that that the optimal $R_{CIP/CGN}$ in terms of the overall preparation efficiency was in the vicinity of 1.0. Herein we selected the CIP–CGN nanoplex prepared at $R_{CIP/CGN} = 1.0$ with CE = 61 ± 0.5%, yield = 42 ± 8%, and CIP loading = 60 ± 9 wt% for the subsequent characterizations and comparison with the CIP–DXT nanoplex.

4.2. Physical characteristics of CIP–CGN nanoplex

The CIP–CGN nanoplex were roughly spherical having size of 59 ± 10 nm as shown in the FESEM image in Fig. 3A with zeta potential of 37 ± 1 mV denoting their colloidal stability. For comparison, the CIP–DXT nanoplex was also roughly spherical, but with a considerably larger size at 380 ± 30 nm (Fig. 3B) and higher zeta potential of 55 ± 15 mV.

The DSC thermographs of the freeze-dried CIP–CGN nanoplex in Fig. 4A showed a broad endothermic peak from ≈25 to 110 °C attributed to (1) the melting of CGN and (2) the moisture evaporation, which was manifested in the slight mass loss in the TGA thermographs shown in Fig. 4B. A sharp melting peak of CGN, which is usually observed between ≈75 and 80 °C (Watase & Nishinari, 1986), however, was not observed in the thermographs of both the CIP–CGN nanoplex and the native CGN in Fig. 4A, because of the overlapping endothermic moisture loss events. The CIP–CGN nanoplex decomposed at ≈225 °C, which was close to the decomposition onset of the native CGN at ≈210 °C, as determined from the extensive mass loss seen in the TGA thermographs and sharp exothermic events in the DSC thermographs. Similar observations were made for the CIP–DXT nanoplex.

PXRD analysis of the nanoplexes after a prolonged storage at 25 °C and 55% relative humidity was carried out to determine their amorphous state stability. The amorphous states of the freshly prepared CIP–CGN and CIP–DXT nanoplexes were first verified by their PXRD patterns in which broad halos characteristic of the amorphous form was observed (data not shown). Most importantly, the amorphous state of the nanoplexes remained unchanged after six-month storage, as confirmed by the broad halos in the PXRD patterns shown in Fig. 4C, in contrast to the sharp peaks observed from the native crystalline CIP.

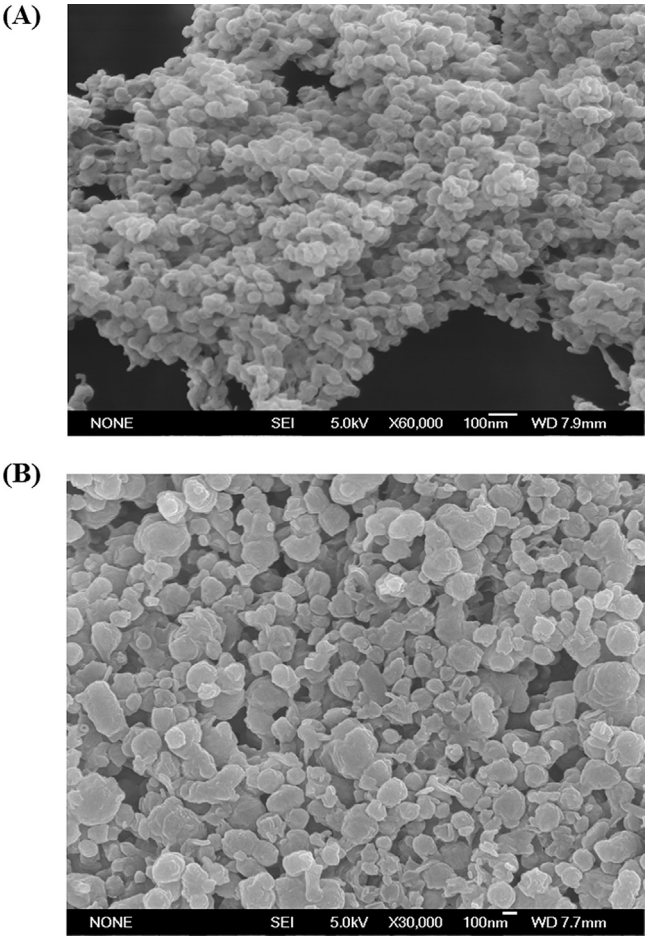

Fig. 3. FESEM image of (A) CIP–CGN nanoplex showing its roughly spherical shape and small size (59 ± 10 nm) and (B) CIP–DXT nanoplex with a larger mean size of 380 ± 30 nm.

4.3. Comparison of CIP–CGN versus CIP–DXT nanoplexes

4.3.1. Preparation efficiency and physical characteristics

The preparation efficiency and physical characteristics of the CIP–CGN and CIP–DXT nanoplexes, where the latter's were reported previously in Cheow and Hadinoto (2012), were compared in Table 1. Both the nanoplexes shared similar optimal preparation conditions, where (1) salt concentration of 0.1 M was found to be ideal above which the salt's charge shielding effect had adverse effects on the nanoplex formation, and (2) the optimal $R_{CIP/DXT}$ or $R_{CIP/CGN}$ was determined to be in the vicinity of 1.0 (i.e. 1.3 for CIP–DXT and 1.0 for CIP–CGN), for the reasons explained earlier in Section 4.1.

Compared to the CIP–CGN nanoplex, the CIP–DXT nanoplex exhibited significantly higher preparation efficiency as reflected in its higher CE (85 ± 2%), yield (74 ± 6%), and CIP loading (80 ± 3 wt%).

Table 1
Preparation efficiency and physical characteristics of the CIP nanoplexes.

	CIP–DXT	CIP–CGN
$R_{CIP/DXT}$ or $R_{CIP/CGN}$	1.3	1.0
Salt conc. (M)	0.1	0.1
CE (%)	85 ± 2	61 ± 0.5
Yield (%)	74 ± 6	42 ± 8
CIP Loading (wt%)	80 ± 3	60 ± 9
Size (nm)	380 ± 30	59 ± 10
Zeta potential (mV)	(−) 55 ± 15	(−) 37 ± 1
Carr's index	17 ± 4	11 ± 0.2

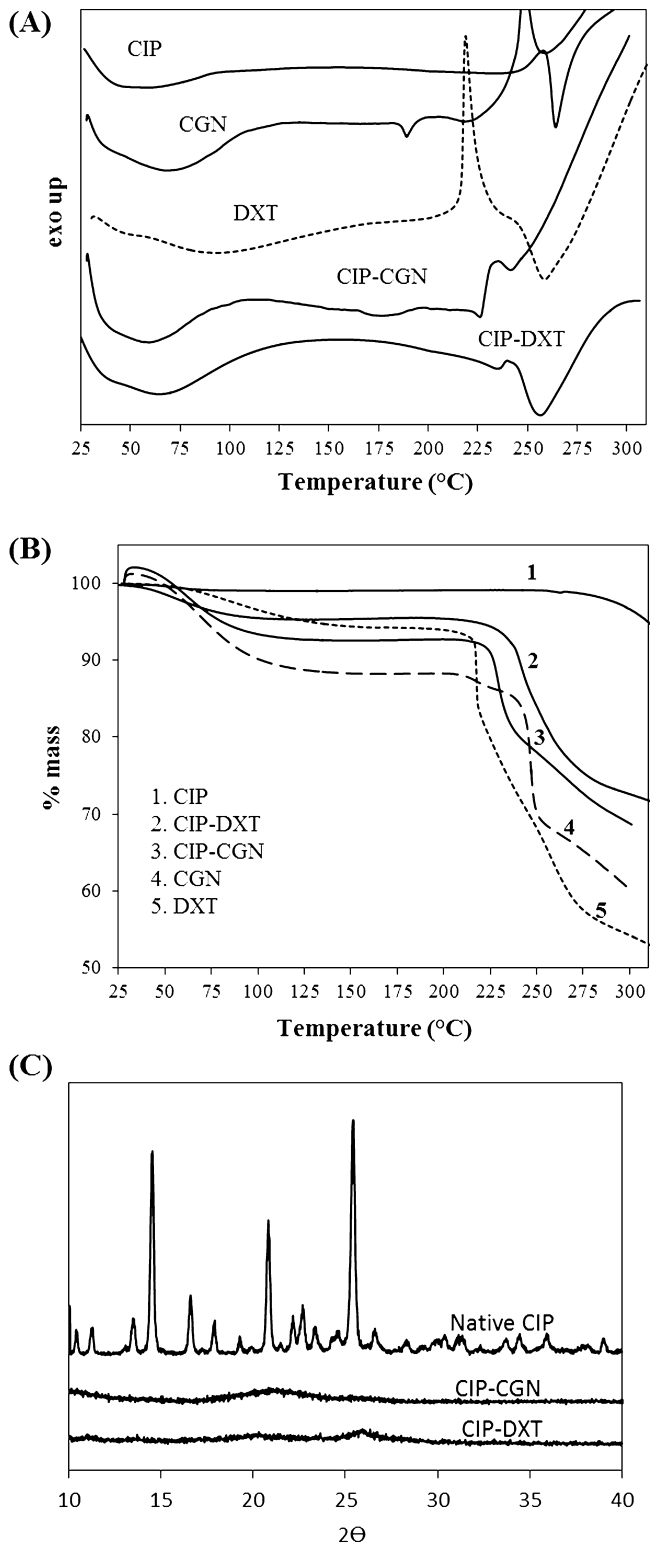

Fig. 4. (A and B) DSC and TGA thermographs showed the broad endothermic peak due to the melting of CGN and moisture evaporation; (C) The amorphous states of the CIP–CGN and CIP–DXT nanoplexes after six-month storage were verified by the PXRD patterns showing the broad halos in contrast to the sharp crystalline peaks of the native CIP.

The higher preparation efficiency of the CIP–DXT nanoplex was attributed to the more than twice higher charge density of DXT compared to that of CGN (i.e. 4.8×10^{-6} versus 2.3×10^{-6} mol charge/mg), resulting in more effective interactions between DXT and the oppositely charged CIP, hence the higher CE and yield. Furthermore, the less effective interactions between CIP and CGN due to the inherently lower charge density of CGN were compounded by the stiffness of the CGN chains, which essentially lowered the local charge density and made the CIP–CGN interaction even less effective, as discussed earlier in the Introduction.

In terms of the physical characteristics, the CIP–CGN nanoplex at 59 ± 10 nm was more than six times smaller than the CIP–DXT nanoplex (380 ± 30 nm) as mentioned earlier. The smaller size indicated that the critical aggregate concentration of the CIP–CGN complex was lower than that of the CIP–DXT complex. In other words, the soluble CIP–CGN complex precipitated to form the nanoplex at an earlier time (i.e. at a lower aggregate concentration) than the CIP–DXT complex. The earlier precipitation of the CIP–CGN complex resulted in fewer complexed CIP molecules, thus a smaller nanoplex size was produced.

The earlier precipitation of the CIP–CGN complex was attributed to the higher hydrophobicity of CGN due to its five-membered cyclic anhydride ether group that was not present in DXT. The higher hydrophobicity increased the tendency of the complex to precipitate out of the solution (Persson, Hugerth, Caram-Lelham, & Sundelof, 2000). Moreover, the smaller CIP–CGN nanoplex size could also be attributed to the lower charge density of CGN, where everything else being equal, the lower charge density of CGN resulted in fewer CIP molecules complexed to CGN than to DXT, thus smaller nanoplex was produced from CIP–CGN complexation.

The CIP–CGN nanoplex was found to have a lower zeta potential than the CIP–DXT nanoplex, which denoted the inferior colloidal stability of the CIP–CGN nanoplex due to the lower charge density of CGN. Despite the differences in their size, colloidal stability, and polysaccharide contents, both nanoplexes were found to exhibit excellent flowability upon their transformation into dry powders as reflected in their Carr's Index values being <21, which signified that they could be readily transformed into oral solid dosage forms.

4.3.2. Supersaturation generation

In the presence of 2 mg/mL HPMC solution in the dissolution medium, the CIP–CGN nanoplex suspension was capable of generating a maximum achievable supersaturation level that reached ≈11× of the CIP saturation solubility (C_{eq} = 0.14 mg/mL) after 20 min, followed by its gradual decrease to ≈6.0× at the equilibrium (Fig. 5A). For comparison, the CIP–DXT nanoplex suspension generated a considerably higher maximum achievable supersaturation level (≈17×), which was reached in shorter time (after 5 min), while exhibiting the same equilibrium supersaturation level of ≈6.0×.

The supersaturation profiles generated by the CIP–CGN and CIP–DXT nanoplex suspensions were typical of amorphous drugs, where the dissolution initially resulted in a highly supersaturated drug concentration significantly above the solubility limit of crystalline drugs. The high supersaturation level subsequently decreased due to the crystallization of the dissolved drug from the supersaturated solution. An equilibrium concentration was eventually reached, where the equilibrium concentration was higher than the crystalline solubility limit of the drug (as seen in the case of the nanoplex), provided that crystallization of the supersaturated drug solution was suppressed, for example, by incorporating HPMC.

The higher maximum achievable supersaturation level exhibited by the CIP–DXT nanoplex suspension was attributed to its faster rate of supersaturation generation, which was owed to the faster CIP dissolution rate from the CIP–DXT nanoplex as shown in Fig. 5B. For comparison, ≈100% of CIP was released from the CIP–DXT nanoplex suspension within 50 min, whereas only ≈70% of CIP was released from the CIP–CGN nanoplex suspension in the same period. This was observed despite the significantly smaller size of the CIP–CGN nanoplex that translated to larger surface areas

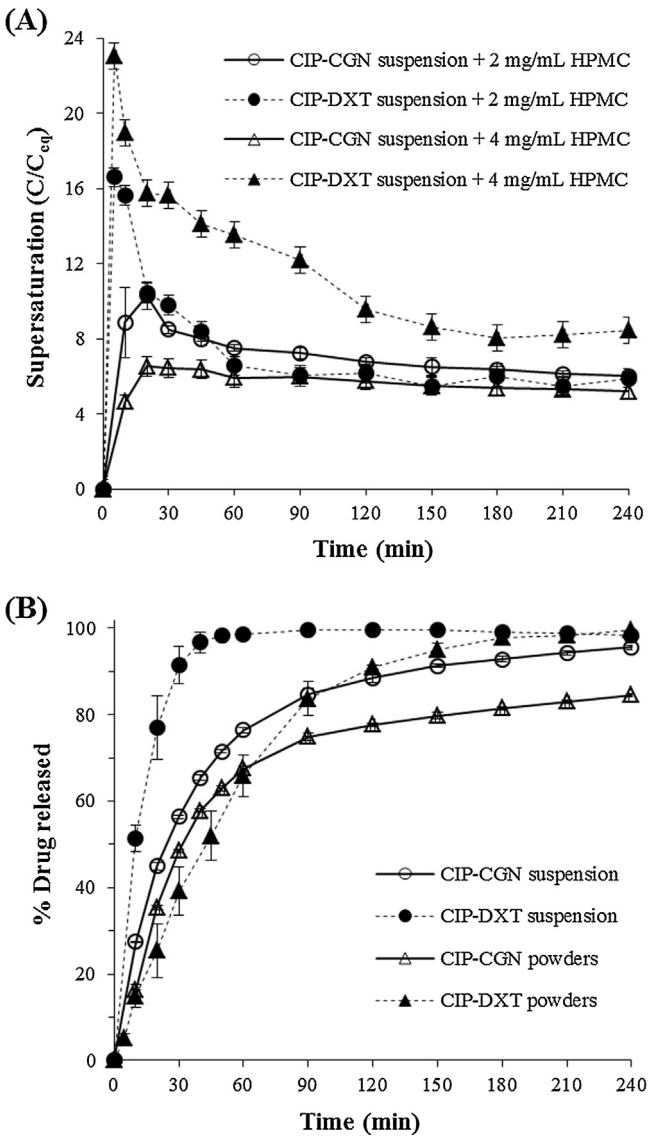

Fig. 5. (A) Supersaturation level generated by the aqueous suspension of CIP–CGN and CIP–DXT nanoplexes in the presence of dissolved HPMC in the dissolution medium at two different concentrations (i.e. 2 and 4 mg/mL); (B) CIP dissolution rate under sink condition as an indicator for the rate of supersaturation generation.

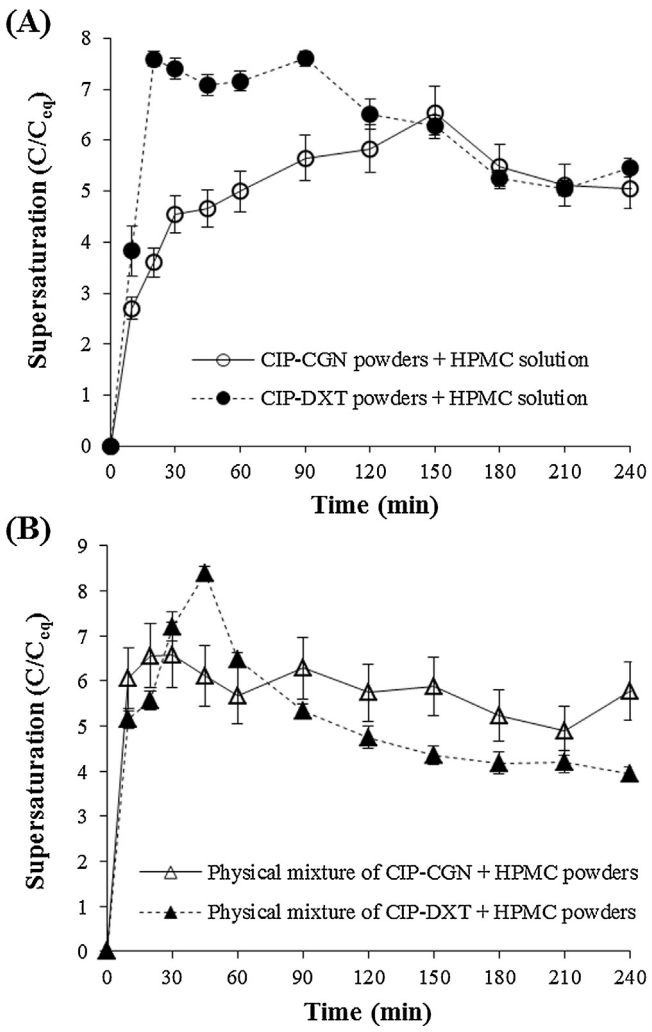

Fig. 6. (A) Supersaturation level generated by CIP–CGN and CIP–DXT nanoplex powders in the presence of dissolved HPMC in the dissolution medium at 2 mg/mL; (B) Supersaturation level generated by CIP–CGN and CIP–DXT nanoplex powders in the presence of physically mixed HPMC powders.

available for dissolution. As a result of the faster CIP dissolution rate, the time window for the remaining solid phase to crystallize was minimized for the CIP–DXT nanoplex suspension, resulting in its higher supersaturation generation.

The slower CIP dissolution rate from the CIP–CGN nanoplex suspension was contributed to by two factors, i.e. (1) the low solubility of CGN in the dissolution medium at 37 °C and (2) the high tendency of CGN to form gel at this temperature, both of which were not applicable to DXT. As CIP decomplexed from CGN in the presence of electrolytes in the dissolution medium, CGN gel (see Supplementary data for the photographic evidence of the gel formation) was formed owed to the high tendency for κ-carrageenan to form gels at this temperature through the double helix model or the domain model (Wang, Rademacher, Sedlmeyer, & Kulozik, 2005). As a result of the CGN gel formation, the freed CIP molecules had to navigate through the gel layer before entering the dissolution medium, resulting in the slower CIP dissolution rate.

When the HPMC concentration in the dissolution medium was raised to 4 mg/mL, the maximum achievable supersaturation level of the CIP–DXT nanoplex suspension was also raised to ≈23×, as the increased presence of HPMC suppressed the crystallization propensity of the dissolved drug and the remaining solid phase to a greater degree (Fig. 5A). In contrast, the CIP–CGN nanoplex suspension generated a lower maximum achievable supersaturation level (≈6.5×) upon increasing the HPMC concentration. In this regard, as CIP decomplexed from the CIP–CGN nanoplex in the dissolution medium, the HPMC present in the dissolution medium was postulated to interact with CGN resulting in diminished outward diffusion of CIP. The slower CIP dissolution rate from the CIP–CGN nanoplex at a higher HPMC concentration led to the lower supersaturation level. The higher HPMC concentration did not adversely impact the supersaturation generation of the CIP–DXT nanoplex because, unlike CGN, DXT was fully soluble in the dissolution medium after CIP decomplexation.

The superior supersaturation generation capability of the CIP–DXT nanoplex was also observed for the dry powder form, albeit at a lower supersaturation level than that of the aqueous suspension form. In the presence of 2 mg/mL HPMC solution, the CIP–DXT nanoplex powders exhibited a maximum achievable supersaturation level of ≈7.6× that was reached after 20 min (Fig. 6A). The supersaturation level was then sustained at the maximum point for additional 70 min, before the supersaturation level gradually decreased to ≈5.0× at the equilibrium. For comparison,

the maximum achievable supersaturation level of the CIP–CGN nanoplex powders was lower at ≈6.3× and was reached in a much slower pace (after 150 min), followed by its immediate decrease to ≈5.0× at the equilibrium.

The superior supersaturation generation ability of the CIP–DXT nanoplex powders was in agreement with the faster dissolution rate observed for the CIP–DXT nanoplex powders as shown in Fig. 5B. For comparison, 100% of CIP was released from the CIP–DXT nanoplex powders after 210 min versus only ≈83% release for the CIP–CGN nanoplex powders in the same period. Nevertheless, the difference in the dissolution rates between the CIP–DXT and CIP–CGN nanoplex powders was not as significant as in their aqueous suspension form, particularly in the early phase of dissolution. This might explain for the higher similarity in the supersaturation profiles between the two nanoplex powders.

Compared to the nanoplex suspension, the lower supersaturation level generated by the nanoplex powders (both CIP–DXT and CIP–CGN) was caused by their slower supersaturation generation rate as can be seen from Fig. 5B. The slower supersaturation generation rate of the nanoplex powders was due to the time needed for them to reconstitute into primary nanoparticles, which required dissolution of the mannitol acting as the interstitial bridges. This time lag in the early phase of dissolution produced smaller surface areas available for dissolution, resulting in the slower CIP dissolution rate for the nanoplex powders.

The superior supersaturation generation capability of the CIP–DXT nanoplex powders, however, was diminished when HPMC was present as dry powders (instead of solution) in the form of physical mixtures of the freeze-dried nanoplex and HPMC powders, which was designed to mimic the HPMC's physical existence in actual solid dosage forms. While the maximum achievable supersaturation level of the CIP–DXT nanoplex powders (≈8.4) remained higher than that of the CIP–CGN nanoplex powders (≈6.5), the former's supersaturation level rapidly decreased upon reaching the maximum point and ended at ≈4× at the equilibrium (Fig. 6B). In contrast, the supersaturation level of the CIP–CGN nanoplex powders was sustained at the maximum point for 210 min after the maximum point was reached.

In this regard, several studies have shown that amorphous drugs that generated prolonged supersaturation at a moderate level in vitro, such as the one demonstrated by the physical mixture of CIP–CGN nanoplex, produced better in vivo bioavailability than those amorphous drugs that generated a high, yet short-lived, supersaturation level, which was similar to the one exhibited by the physical mixture of CIP–DXT nanoplex (Augustijns & Brewster, 2012). Not unexpectedly, the calculated area under the curve (AUC) in the time versus concentration plot in Fig. 6B was found to be slightly larger for the physical mixture of CIP–CGN nanoplex at ≈1355 × C_{eq} mg/mL.min compared to ≈1213 × C_{eq} mg/mL.min for the physical mixture of CIP–DXT nanoplex. The calculated AUC, which is typically used as in vitro indicator for bioavailability (Sun & Lee, 2013), thus indicated the superiority of the physical mixture of the CIP–CGN nanoplex in generating the supersaturation.

Compared to the supersaturation generation in the presence of dissolved HPMC, the inherently slow-dissolving nature of HPMC (Siepmann, Kranz, Bodmeier, & Peppas, 1999) in the physical mixtures rendered HPMC less effective in suppressing the solution-mediated crystallization of the dissolved drug. The faster supersaturation generation rate of the CIP–DXT nanoplex powders caused them to possess a higher crystallization propensity than the CIP–CGN nanoplex powders due to the higher supersaturation level generated in the former. In the absence of HPMC in the dissolution medium, the highly supersaturated solution rapidly crystallized resulting in the lower AUC for the physical mixture of CIP–DXT nanoplex.

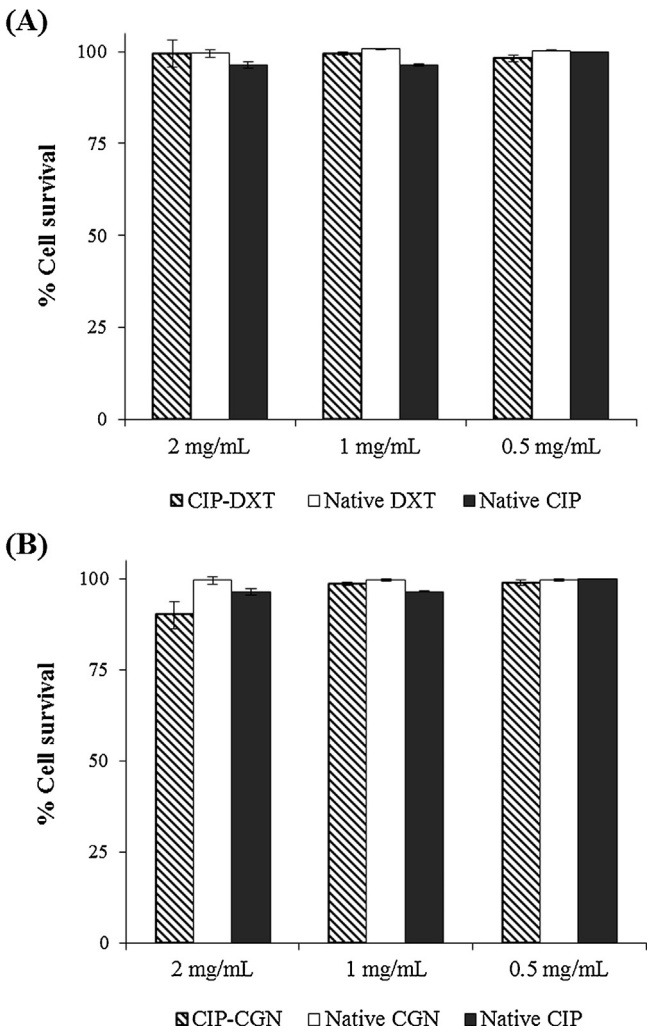

Fig. 7. in vitro cytotoxicity of (A) CIP–DXT and (B) CIP–CGN nanoplexes towards the A549 cells at three different exposure levels (i.e. 0.5, 1, and 2 mg/mL).

Thus, a better HPMC incorporation method (other than physical mixing), which can circumvent the issue of slow-dissolving nature of HPMC, is needed in the solid dosage form preparation step for us to be able to fully exploit the superior supersaturation generation capability of the CIP–DXT nanoplex. To this end, simultaneous drying of the nanoplex with HPMC by either spray or freeze drying is currently being investigated in our laboratory as a potential solid dosage form formulation strategy for the CIP–DXT nanoplex.

4.3.3. *Antimicrobial activity and cytotoxicity*

The CIP–DXT and CIP–CGN nanoplexes were found to possess the same MIC values (0.25 μL/g) against *E. coli* bacteria indicating their similar antimicrobial activities. Importantly, the MIC of the nanoplex was found to be identical to that of the native CIP, which suggested that the antimicrobial activity of the antibiotic was not affected by the electrostatic complexation with polysaccharides, nor was the antimicrobial activity of CIP affected by the high temperature (60 °C) used in the CIP–CGN nanoplex preparation. Likewise, both nanoplexes were found to exhibit minimal cytotoxicity toward the A549 cells in the range of CIP concentration investigated (Fig. 7), which suggested that the polysaccharides and the native drug remained non-cytotoxic after being transformed into the nanoplex. Thus, in terms of the antimicrobial activity and cytotoxicity, there was minimal difference between the CIP–DXT and CIP–CGN nanoplex.

5. Conclusion

Our study showed that using CGN as the polysaccharides (in place of DXT) to prepare amorphous nanodrugs of CIP by drug-polysaccharide electrostatic complexation resulted in (1) lower preparation efficiency, (2) vastly smaller size, and (3) inferior supersaturation generation capability. First, the lower preparation efficiency of the CIP–CGN nanoplex was due to the lower charge density and chain flexibility of CGN compared to DXT, which resulted in less effective electrostatic interactions between the drug and the polysaccharides. Despite the variation in their preparation efficiency, the CIP–CGN and CIP–DXT nanoplexes, which were both colloidally stable, shared similar optimal preparation conditions in terms of the optimal drug-to-polysaccharide charge ratio and salt concentration. In addition, they also shared similar trends in the yield and CIP loading variations upon the change in the drug-to-polysaccharide charge ratio.

Second, the lower charge density of CGN, which resulted in lower CIP loading, was also responsible for the small size of the CIP–CGN nanoplex, where coupled with the higher hydrophobicity of CGN, they expedited the onset of precipitation of the drug-polysaccharide complex. Third, the inferior supersaturation generation capability of the CIP–CGN nanoplex was caused by its slower CIP dissolution rate (despite its smaller size) due to the low solubility and high gelation tendency of CGN at 37 °C. The slower CIP dissolution rate increased the time window for the remaining solid phase to crystallize, resulting in the lower supersaturation generation.

Last but not least, both nanoplexes were found to be non-cytotoxic and preserved the antimicrobial activity of the native drug, as well as their amorphous state. These findings clearly pointed out that the CIP–DXT nanoplex was superior to the CIP–CGN nanoplex in all the aspects investigated. However, a better HPMC incorporation method to prepare the solid dosage form, other than physically mixing HPMC with the nanoplex powders, is needed to fully exploit the superior supersaturation generation capability of the CIP–DXT nanoplex.

Acknowledgement

The authors would like to acknowledge the funding from GlaxoSmithKline Singapore under their 2013 Green and Sustainable Pharmaceutical Manufacturing initiative (PI: Kunn Hadinoto Ong).

Appendix A. Supplementary data

Supplementary data associated with this article can be found, in the online version, at doi:10.1016/j.carbpol.2014.10.015.

References

Alonzo, D., Zhang, G., Zhou, D., Gao, Y., & Taylor, L. (2010). Understanding the behavior of amorphous pharmaceutical systems during dissolution. *Pharmaceutical Research*, *27*(4), 608–618.

Ando, H. Y., & Radebaugh, G. W. (2005). Property-based drug design and preformulation. In D. B. Troy (Ed.), *Remington: The science and practice of pharmacy*. Philadelphia, PA: Lippincott Williams & Wilkins.

Augustijns, P., & Brewster, M. E. (2012). Supersaturating drug delivery systems: Fast is not necessarily good enough. *Journal of Pharmaceutical Sciences*, *101*(1), 7–9.

Caram-Lelham, N., Hed, F., & Sundelof, L. O. (1997). Adsorption of charged amphiphiles to oppositely charged polysaccharides—A study of the influence of polysaccharide structure and hydrophobicity of the amphiphile molecule. *Biopolymers*, *41*(7), 765–772.

Cheow, W. S., & Hadinoto, K. (2012). Self-assembled amorphous drug-polyelectrolyte nanoparticle complex with enhanced dissolution rate and saturation solubility. *Journal of Colloid and Interface Science*, *367*, 518–526.

Cheow, W. S., Kiew, T. Y., Yang, Y., & Hadinoto, K. (2014). Amorphization strategy affects the stability and supersaturation profile of amorphous drug nanoparticles. *Molecular Pharmaceutics*, *11*(5), 1611–1620.

Delair, T. (2011). Colloidal polyelectrolyte complexes of chitosan and dextran sulfate towards versatile nanocarriers of bioactive molecules. *European Journal of Pharmaceutics and Biopharmaceutics*, *78*(1), 10–18.

Dhumal, R. S., Biradar, S. V., Yamamura, S., Paradkar, A. R., & York, P. (2008). Preparation of amorphous cefuroxime axetil nanoparticles by sonoprecipitation for enhancement of bioavailability. *European Journal of Pharmaceutics and Biopharmaceutics*, *70*(1), 109–115.

Hugerth, A., & Sundelof, L. O. (2001). The effect of polyelectrolyte counterion specificity, charge density, and conformation on polyelectrolyte-amphiphile interaction: The carrageenan/furcellaran amitriptyline system. *Biopolymers*, *58*(2), 186–194.

Kara, S., Tamerler, C., & Pekcan, O. (2003). Cation effects on swelling of k-carrageenan: A photon transmission study. *Biopolymers*, *70*(2), 240–251.

Li, L., Ni, R., Shao, Y., & Mao, S. R. (2014). Carrageenan and its applications in drug delivery. *Carbohydrate Polymers*, *103*, 1–11.

Lindfors, L., Skantze, P., Skantze, U., Rasmusson, M., Zackrisson, A., & Olsson, U. (2006). Amorphous drug nanosuspensions. 1. Inhibition of Ostwald ripening. *Langmuir*, *22*(3), 906–910.

Matteucci, M. E., Brettmann, B. K., Rogers, T. L., Elder, E. J., Williams, R. O., & Johnston, K. P. (2007). Design of potent amorphous drug nanoparticles for rapid generation of highly supersaturated media. *Molecular Pharmaceutics*, *4*(5), 782–793.

Mou, D. S., Chen, H. B., Wan, J. L., Xu, H. B., & Yang, X. L. (2011). Potent dried drug nanosuspensions for oral bioavailability enhancement of poorly soluble drugs with pH-dependent solubility. *International Journal of Pharmaceutics*, *413*(1–2), 237–244.

Persson, B., Hugerth, A., Caram-Lelham, N., & Sundelof, L. O. (2000). Dextran sulfate-amphiphile interaction; effect of polyelectrolyte charge density and amphiphile hydrophobicity. *Langmuir*, *16*(2), 313–317.

Ramasamy, T., Tran, T. H., Cho, H. J., Kim, J. H., Kim, Y. I., Jeon, J. Y., et al. (2014). Chitosan-based polyelectrolyte complexes as potential nanoparticulate carriers: Physicochemical and biological characterization. *Pharmaceutical Research*, *31*(5), 1302–1314.

Schatz, C., Domard, A., Viton, C., Pichot, C., & Delair, T. (2004). Versatile and efficient formation of colloids of biopolymer-based polyelectrolyte complexes. *Biomacromolecules*, *5*(5), 1882–1892.

Siepmann, J., Kranz, H., Bodmeier, R., & Peppas, N. A. (1999). HPMC-matrices for controlled drug delivery: A new model combining diffusion, swelling, and dissolution mechanisms and predicting the release kinetics. *Pharmaceutical Research*, *16*(11), 1748–1756.

Slootmaekers, D., Dejonghe, C., Reynaers, H., Varkevisser, F. A., & Vantreslong, C. J. B. (1988). Static light-scattering from kappa-carrageenan solutions. *International Journal of Biological Macromolecules*, *10*(3), 160–168.

Sun, D. J. D., & Lee, P. I. (2013). Evolution of supersaturation of amorphous pharmaceuticals: The effect of rate of supersaturation generation. *Molecular Pharmaceutics*, *10*(11), 4330–4346.

Tajarobi, F., Larsson, A., Matic, H., & Abrahmsen-Alami, S. (2011). The influence of crystallization inhibition of HPMC and HPMCAS on model substance dissolution and release in swellable matrix tablets. *European Journal of Pharmaceutics and Biopharmaceutics*, *78*(1), 125–133.

Vandeloosdrecht, A. A., Beelen, R. H. J., Ossenkoppele, G. J., Broekhoven, M. G., & Langenhuijsen, M. (1994). A tetrazolium-based colorimetric MTT assay to quantitate human monocyte mediated cytotoxicity against leukemic-cells from cell-lines and patients with acute myeloid-leukemia. *Journal of Immunological Methods*, *174*(1–2), 311–320.

Wang, Q., Rademacher, B., Sedlmeyer, F., & Kulozik, U. (2005). Gelation behaviour of aqueous solutions of different types of carrageenan investigated by low-intensity-ultrasound measurements and comparison to rheological measurements. *Innovative Food Science & Emerging Technologies*, *6*(4), 465–472.

Watase, M., & Nishinari, K. (1986). Rheology, DSC, and volume or weight change induced by immersion in solvents for agarose and kappa-carrageenan gels. *Polymer Journal*, *18*(12), 1017–1025.

Zheng, J. (2009). *Formulation and analytical development for low-dose oral drug products*. New Jersey: John Wiley and Sons.